Transient 3-Dimensional Behavior of Gas-Solid Fluidization Measured Using Electrical Capacitance Volume Tomography (ECVT)

Bing Du, W. Warsito and Liang-Shih Fan
Department of Chemical and Biomolecular Engineering, The Ohio State University
140 West 19th Avenue, Columbus, OH 43210

Introduction

The transient flow behavior in the gas-solid fluidization system is complex. Although numerous experimental and theoretical studies have been conducted on this system, its real time, 3-dimensional flow structures are still far from full comprehension. The common measurement techniques using probes such as the optical fiber probe or the capacitance probe can only provide the local point flow properties in the bed. It is challenging, however, to develop non-intrusive techniques that are capable of performing real-time, 3-dimensional imaging of the multiphase flow field. This study reports the development of the first Electrical capacitance volume tomography (ECVT) and its applications to the 3-D non-intrusive measurements of the dynamic behavior of a gas-solid fluidized bed.

3D ECVT with NN-MOIRT

The ECVT involves tasks of collecting capacitance data from electrodes placed around the wall outside the vessel and reconstructing image based on the measured capacitance data. The capacitance is measured based on the Poison equation which can be written in three-dimensional space as:

$$\nabla \cdot e(x,y,z)\nabla\phi(x,y,z) = -\rho(x,y,z) \tag{1}$$

where $e(x,y,z)$ is the permittivity distribution; $\phi(x,y,z)$ is the electrical field distributions; $\rho(x,y,z)$ is the charge density. The measured capacitance C_i of the i-th pair between the source and the detector electrodes is obtained by integrating Eq. (1):

$$C_i = -\frac{1}{\Delta V_{ij}} \oiint_{A_i} e(x,y,z)\nabla\phi(x,y,z)dA \tag{2}$$

where ΔV_i is the voltage difference between the electrode pair; A_i is the surface area enclosing the detector electrode. Equation (2) relates the dielectric constant (permittivity) distribution, $e(x,y,z)$, to the measured capacitance C_i.

The image reconstruction process is an inverse problem involving the estimation of the permittivity distribution from the measured capacitance data. Since there is no analytical method for the non-linear inverse problem, linearization using the so-called sensitivity model is commonly applied (Huang et al., 1989; Xie et al., 1992). The sensitivity map is constructed by filling the j-th voxel with high permittivity and the rest is material of low permittivity, and solving numerically Eq. (2) based on the finite element method (FEM) using the OPERA-3D TOSCA software package (Vector Fields, 2001). For imaging a three-dimensional object, the sensitivity matrix has to have a three-dimensional variation, especially in the axial (z-axis) direction to differentiate the depth along the sensor length. Based on the sensitivity model, Eq. (2) then can be written in matrix expression as:

$$\mathbf{C} = \mathbf{SG} \tag{3}$$

where **C** is the M-dimension capacitance data vector; **G** is *N*-dimension image vector; *N* is the number of voxels in three-dimensional image; and *M* is the number of electrode-pair combinations. Specifically, *N* is equal to $n \times n \times n_L$, where *n* is the number of voxel in one side of image frame (layer); n_L is the number of layer). The 3D volume image digitization is shown on bottom-left of Figure 1. The sensitivity matrix S has a dimension of *M X N*.

The reconstruction problem involves finding methods for estimating the image vector **G** from the measurement vector **C**, and to minimize the error between the estimated and the predicted capacitance, **C** under certain conditions (criteria), such that

$$\mathbf{SG} \leq \mathbf{C} \qquad (4)$$

The image reconstruction is an ill-posed problem, i.e. there are fewer independent measurements than unknown pixel values. Therefore, there is no unique solution for the inverse problem. There may be more than one or many possible estimations (answers). How close the estimation to the exact answer definitely depends on the definition of the error and the image algorithm. This is a common problem for all tomography reconstruction techniques. What we can do in an image reconstruction, which is not restricted to ECVT, is "to estimate an image vector (permittivity distribution in ECVT) from the measurement data (capacitance data in ECT), and minimize the error" (Herman, 1980). In ECVT, the error is defined as the difference between the measured capacitance data and the capacitance value calculated from estimated permittivity distribution. An iterative approach is usually employed to update the estimated permittivity distribution until maximum allowable error is reached. However, one single criterion such as the least square error as used in most kinds of iterative reconstruction techniques (Yang and Peng, 2003) does not necessarily give rise to the accurate image, since the least squared criterion does not contain any information concerning the nature of a 'desirable' solution. Therefore, more than one objective function is required to be considered simultaneously in order to choose the 'best compromise solution' or the best probability of the answer among possible alternatives. The probability problem even worsens for noise containing capacitance data. Multi-criterion optimization using more than one objective function is required to reduce the possibility of alternative solutions, and hence reducing the non-uniqueness of the problem in obtaining a more definitive solution.

In this study, a multi-criterion optimization based image reconstruction technique developed earlier by the authors (Warsito and Fan, 2001) for solving the inverse problem for the 2D ECT is extended to solve the inverse problem for the 3D ECVT. A modified Hopfield neural network (Hopfield and Tank, 1985) is invoked to solve the optimization problem by minimizing the four objective functions: negative entropy function, least square errors, smoothness and small peakedness function, and 3D-to-2D matching function. The 3D ECVT image reconstruction is accomplished by introducing the 3D sensitivity matrix (Eq. (4)) into the NN-MOIRT algorithm. The image is reconstructed into a three-dimensional image (volume image) consisting of image voxels (volume pixels) in a number of frames (layers) instead of a single frame as in two-dimensional image reconstruction. The NN-MOIRT algorithm reconstructs simultaneously the volume image into 20×20×20 voxels from 276 capacitance data based on 12-electrode twin-plane sensor for simulation and 66 capacitance data obtained from 6-electrode twin-plane sensor for actual measurement. The details on the algorithm is described elsewhere (Warsito and Fan, 2001, 2003, 2005). The implementation of more than one objective functions thus yields a higher probability of obtaining an accurate solution (estimation) in the image reconstruction. This is especially the case for 3D reconstruction as

there are much more number of voxels from the limited measurement data, i.e. there are 6160 unknown permittivity inside the domain from only 66 or 276 available capacitance data.

Figure 1 (first row) shows the three-dimensional reconstruction results of a sphere based on simulated capacitance data obtained by solving Eq. (2) given permittivity distribution of the objects. The second row of the figure shows a half portion of the sphere when entering the top part of the sensor. The diameter of the sphere is 0.5 of the diameter of the sensor which equals the whole dimension of the image. Excellent agreements between the

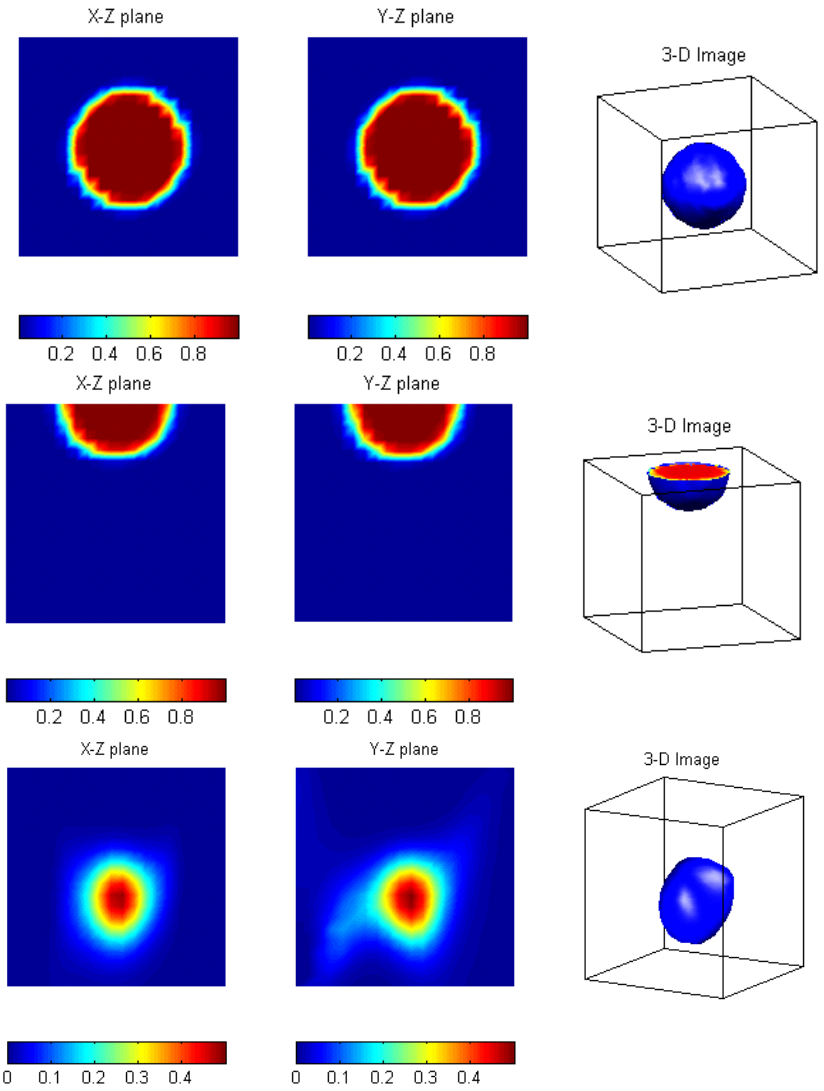

Figure 1 Reconstruction results of the dielectric, spherical model objects: diameter = 0.5D_0 (top), the model object of one-half sphere: diameter = 0.5D_0 (middle), an actual dielectric sphere: diameter = 0.25D_0 (bottom)

reconstructed 3D images and the model objects are obtained in both images. The reconstruction results from actual measurement data are shown in the bottom row in Fig. 1 using a spherical dielectric object with a diameter of 2.5 cm and a capacitance sensor with an inner diameter of 10 cm. The object is tethered to a thin non-conductive rope and is moving within the sensor. The sensor used for the actual measurement is a 6-electrode twin-plane

sensor, less number of electrodes than the one used for simulated measurement as in Fig. 1. Despite the use of fewer electrodes, and hence a higher scanning rate, it can be seen from Fig. 1 that a clear image can still be obtained even though some distortions from the original spherical shape are observed due to noise which is measured up to 20% (SNR about 30dB).

Experiments

The ECT comprises the capacitance sensor, sensing electronics for data acquisition, and a computer system for image reconstruction. The capacitance sensor array is a twin plane sensor using 6 electrodes for each plane. The geometry of the sensor is not necessarily of a rectangular shape as commonly employed for the 2-D ECT. The design of a sensor that provides distinct radial and axial variations in the electric field is critical for accurate measurements using the ECVT. In the flow experiments, the center of sensor is located at 20 cm above the distributors. The length of each electrode is 8 cm and thus, the total interrogation volume is 16 cm in length. The data acquisition system is from Process Tomography Limited (UK) and is capable of capturing image data up to 80 frames per second. There are 66 combinations of independent capacitance measurements between electrode pairs from 12 electrodes arranged in two planes. The image reconstruction and data post-processing are run on a Pentium 4 machine, 3 GHz and a memory of 2 GB.

A fluidized bed of 0.1 m ID and 1.9 m in height with a porous plate distributor with a pore size of 20 μm and a fractional free area of 60% is employed in this study. A two-stage cyclone separates gas and particles and is installed in the freeboard of each fluidized bed. Details of the experimental setup have been reported elsewhere (Du et al., 2002). Both of the Geldart Group A particles (FCC catalyst with a mean diameter of 60 μm and a density of 1400 kg/m^3) and Group B particles (glass beads with a mean diameter of 200 μm and a density of 2500 kg/m^3) are employed in the experiments.

Sample Results and Concluding Remarks

Figure 2 shows the 3-dimensional image a bubble in a gas-solid fluidized bed with 200 μm glass beads at a gas velocity of 0.2 m/s. A bubble with spherical cap shape is clearly observed by the ECVT technique. Based on the time series of the 3D images of the gas-solid fluidized bed, the dynamic flow characteristics of the bubbles including the bubble size and bubble velocity, and the flow pattern of the particles around the

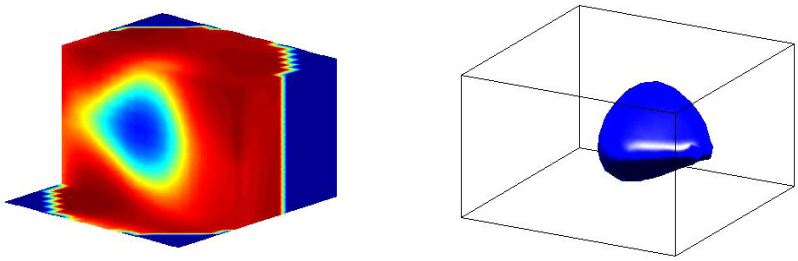

Figure 2 3-dimensional image of a bubble in a gas-solid fluidized bed with 200 μm glass beads at a gas velocity of 0.2 m/s

bubbles can be illustrated. The flow behavior of the voids in the turbulent regime can also be obtained by the 3D images obtained from the ECVT.

References

Du, B., Fan, L.S., Wei, F. & Warsito, W. (2002). Gas and solids mixing behavior in a turbulent fluidized bed. American Institute of Chemical Engineers Journal, 48, 1896-1909.

Herman, G.T. (1980). Image reconstruction from projections, Academic Press, NY, USA.

Hopfield, and Tank, D. (1985). 'Neural' computation of decisions in optimization problems. Biol. Cybern., 52, 141-152.

Huang, S.M., Plaskowski, A., Xie, C.G. & Beck, M.S. (1989) Tomographic imaging of two-component flow using capacitance sensors. Journal of Physics E: Science, 173-177.

Vector Fields, Inc. (2001). OPERA-3D Software for Electromagnetic Design, Vector Fields Inc., Aurora, IL, USA.

Warsito, W. and Fan, L.-S. (2001). Neural network based multi-criteria optimization image reconstruction technique for imaging two- and three-phase flow systems using electrical capacitance tomography. Measurement Science and Technology, 12, 2198-2210.

Warsito, W. & Fan, L.-S. (2003). Neural network multi-criteria optimization image reconstruction technique (NN-MOIRT) for linear and non-linear process tomographic imaging of two- and three-phase flow systems. Chemical Engineering and Processing 42, 663-674.

Warsito,W. & Fan, L.S. (2005). Dynamics of spiral bubble plume motion in the entrance region of bubble columns and three-phase fluidized beds using 3D ECT. Chemical Engineering Science, 60, 6073-6084.

Xie, C.G., Huang, S.M., Hoyle, B.S., Thorn, R., Lean, C., Snowden, D. & Beck, M.S. (1992) Electrical capacitance tomography for flow imaging system model for development of image reconstruction algorithms and design of primary sensor. IEE Proceedings G, 139, 89-98.

Yang, W.Q., & Peng, L. (2003). Image reconstruction algorithms for electrical capacitance tomography. Measurement Science and Technology, 14, R1–R13.